Transp Porous Med (2012) 94:759–774
DOI 10.1007/s11242-012-0023-z

Conjugate Natural Convection in a Porous Enclosure with Non-Uniform Heat Generation

H. Saleh · I. Hashim

Received: 31 January 2012 / Accepted: 8 May 2012 / Published online: 24 May 2012

Abstract Effects of a conductive wall on natural convection in a square porous enclosure having internal heating at a rate proportional to a power of temperature difference is studied numerically in this article. The horizontal heating is considered, where the vertical walls heated isothermally at different temperatures while the horizontal walls are kept adiabatic. The Darcy model is used in the mathematical formulation for the porous layer and finite difference method is applied to solve the dimensionless governing equations. The governing parameters considered are the Rayleigh number ($0 \leq Ra \leq 1000$), the internal heating and the local exponent parameters ($0 \leq \gamma \leq 5$), ($1 \leq \lambda \leq 3$), the wall to porous thermal conductivity ratio ($0.44 \leq Kr \leq 9.9$) and the ratio of wall thickness to its width ($0.02 \leq D \leq 0.5$). The results are presented to show the effect of these parameters on the fluid flow and heat transfer characteristics. It is found a strong internal heating can generate significant maximum fluid temperature more than the conductive solid wall. Increasing value thermal conductivity ratio and/or decreasing the thickness of solid wall can increase the maximum fluid temperature. It is also found that at very low Rayleigh number, the heat transfer across the porous enclosure remain stable for any values of the thermal conductivity ratio.

Keywords Conjugate heat transfer · Natural convection · Darcy's law · Finite difference method

H. Saleh (✉)
School of Mathematical Sciences, Universiti Kebangsaan Malaysia, 43600 UKM, Bangi, Selangor, Malaysia
e-mail: Dr.habibissaleh@gmail.com

I. Hashim
Centre for Modelling & Data Analysis, School of Mathematical Sciences, Universiti Kebangsaan Malaysia, 43600 UKM, Bangi, Selangor, Malaysia
e-mail: ishak_h@ukm.my

List of Symbols

Variables

d, D	Wall thickness, dimensionless wall thickness
g	Gravitational acceleration
G	Measure of the internal heat generation
K	Permeability of the porous medium
Kr	Thermal conductivity ratio
k_{p}	Effective thermal conductivity of porous medium
k_{w}	Thermal conductivity of wall
ℓ	Width and height of enclosure
$\overline{Nu}$	Average Nusselt number
Ra	Rayleigh number
T	Temperature
u, v	Velocity components in the x- and y-directions
x, y and X, Y	Space coordinates and dimensionless space coordinates

Greeks

α	Effective thermal diffusivity
β	Thermal expansion coefficient
γ	Internal heating parameter
λ	Local heating exponent
ψ, Ψ	Stream function, dimensionless stream function
Θ	Dimensionless temperature
ν	Kinematic viscosity

Subscripts

c	Cold
h	Hot
max	Maximum
p	Porous
w	Wall

1 Introduction

Fluid flows in porous media has occupied the central stage in many fundamental heat transfer analysis and has received considerable attention over the last few decades. This interest is due to its wide range of applications, for example, high performance insulation for buildings, chemical catalytic reactors, packed sphere beds, grain storage and such geophysical problems as frost heave. Porous media are also of interest in relation to the underground spread of pollutants, solar power collectors, and to geothermal energy systems. The literature concerning convective flow in porous media is abundant and representative studies in this may be found in the recent books by Ingham and Pop (1998), Pop and Ingham (2001), Ingham et al. (2004), Ingham and

Pop (2005), Vafai (2005), Nield and Bejan (2006), de Lemos (2006), and Vadasz (2008).

Analysis of the convective flows within the porous materials when the porous material provides its own source of heat has become a separate topic for research in last 30 years. This interest is due to its importance in various engineering applications, such as spontaneous combustion in coal stockpiles, heat removal from nuclear fuel debris in nuclear reactors, underground disposal of radioactive waste materials, and exothermic chemical reactions in packed-bed reactors. Moreover, this phenomenon can be encountered during the storage of agricultural products where heat is generated as a result of metabolism of the products. Convective flows are governed by non-linear partial differential equations, which represent conservation laws for the mass, momentum, and energy. Numerical treatment usually used to solve the equations or if possible by an analytic method. Numerical investigation of natural convection in porous enclosure having uniform internal heating firstly conducted by Haajizadeh et al. (1984). Then continued by Rao and Wang (1991) and analytically by Joshi et al. (2006). Recently, Mealey and Merkin (2009) moved away from the study of uniform internal heating to that of non-uniform internal heating and solved the problem numerically and analytically. They found that a strong non-uniform internal heating can generate significant maximum fluid temperatures above the heated wall.

In some situations of considerable practical importance, the heated or cooled wall thickness is finite having a thermal conductivity significantly different with the fluids in the porous material. This gives an alternative way in which a convective flow can be set up within the porous material. Such a situation can arise in the high performance insulation for buildings or the heated ground water. For example, in the heated ground water due to hot intrusion may rise in a narrow fractured zone, as the heated water rises, it eventually encounters a cooler rock formation that sandwiches the permeable vertically slender space. This causes heat transfer between the hot water and the colder surrounding rocks. This coupled conduction–convection problem is known as conjugate convection. Conjugate natural convection in a rectangular porous enclosure surrounded by walls was firstly examined by Chang and Lin (1994a). Their results show that wall conduction effects decrease the overall heat transfer rate from the hot to cold sides of the system. Chang and Lin (1994b) also studied the effect of wall heat conduction on natural convection in an enclosure filled with a non-Darcian porous medium. Baytas et al. (2001) gave a numerical analysis in a square porous enclosure bounded by two horizontal conductive walls. Later, Saeid (2007a) studied conjugate natural convection in a square porous enclosure with two equal-thickness walls. Saeid (2007b) investigated the case when only one vertical wall is of finite thickness. Thermal non-equilibrium model to investigate the conjugate natural convection in porous media was reported by Saeid (2008). Varol et al. (2008) studied a porous enclosure bounded by two solid massive walls from vertical sides at different thicknesses. Al-Amiri et al. (2008) considered the two insulated horizontal walls of finite thickness and used the Forchheimer–Brinkman-extended Darcy model in the mathematical formulation. Very recently, Varol et al. (2010) and Saleh et al. (2011) analyzed convective flows of the Darcy-Bénard convection in a thick bottom-walled enclosure.

Interaction between a conduction wall and a convection in a porous enclosure having internal heat generation has not received attention. Therefore, this study examines the effect of the conductive heated wall on natural convection in a square enclosure filled with a fluid-saturated porous medium having non-uniform internal heating. Flow development, temperature distribution, and the heat transfer rate across the wall and porous enclosure will be presented graphically.

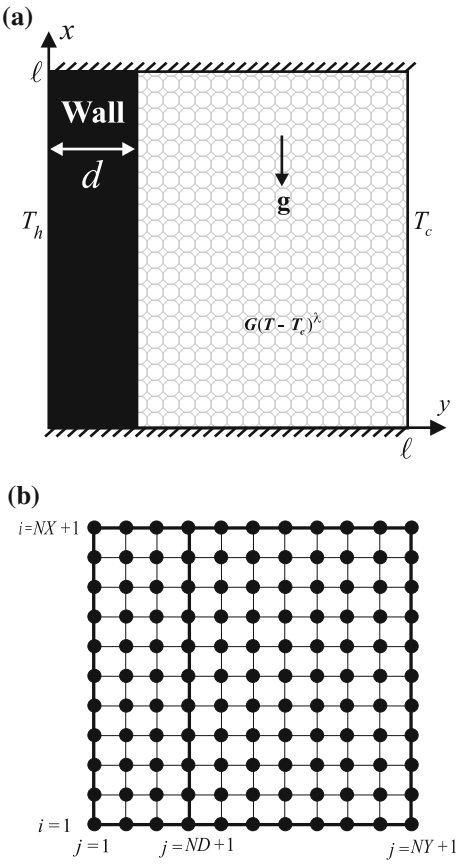

Fig. 1 **a** Schematic representation of the model, **b** Grid-points distribution in the conducting wall ($j \leq ND+1$) and porous ($j > ND+1$)

2 Mathematical Formulation

A schematic diagram of horizontal heating of a porous enclosure with finite wall thickness is shown in Fig. 1a. The choice of the spatial coordinates is also described in this figure, where the gravitational field is parallel to the x-axis. The left surface ($y = 0$) of the impermeable wall is heated to a constant temperature T_{h}, and the right surface ($y = 0$) of the porous enclosure is cooled to a constant temperature T_{c} while the horizontal walls are kept adiabatic. Heat is assumed also to be generated internally within the porous medium at a rate proportional to $(T_{\mathrm{p}} - T_{\mathrm{c}})^{\lambda} (\lambda \geq 1)$. This relation, as explained by Mealey and Merkin (2009), is an approximation of the state of some exothermic chemical reaction. The Oberbeck-Boussinesq approximation is used and the fluid and the porous matrix are in local thermal equilibrium.

With these assumptions, the continuity, momentum, and energy equations for steady, two-dimensional flow in an isotropic and homogeneous porous medium are

$$\frac{\partial u}{\partial x} + \frac{\partial v}{\partial y} = 0 \tag{1}$$

$$\frac{\partial u}{\partial y} - \frac{\partial v}{\partial v} = \frac{gK\beta}{\nu} \frac{\partial T_{\mathrm{p}}}{\partial y} \tag{2}$$

$$u\frac{\partial T_{\mathrm{p}}}{\partial x}-v\frac{\partial T_{\mathrm{p}}}{\partial y}=\alpha\left(\frac{\partial^2 T_{\mathrm{p}}}{\partial x^2}+\frac{\partial^2 T_{\mathrm{p}}}{\partial y^2}\right)+\frac{G(T_{\mathrm{p}}-T_{\mathrm{c}})^{\lambda}}{\rho c_{\mathrm{p}}} \tag{3}$$

and the energy equation for the impermeable wall is

$$\frac{\partial^2 T_{\mathrm{w}}}{\partial x^2}+\frac{\partial^2 T_{\mathrm{w}}}{\partial y^2}=0 \tag{4}$$

where the subscript p for porous layer and w for the wall. The above equations correspond to having the porous medium modeled according to Darcy's law. Because of the complexity of pore geometries in a porous medium, Darcy's law has to be used to obtain any meaningful insights into the physics of flow in porous media. Darcy's law has been verified by the results of many experiments. Theoretical backing for it has been obtained in various ways, with the aid of either deterministic or statistical models (Nield and Bejan 2006). Vafai (2005) have described that Darcy approximation is reasonable for the geothermal flows, except perhaps near boreholes (Vafai 2005). Darcy's law is valid only when the pore Reynolds number is of the order of 1 and for many practical applications, Darcy's law is not valid, and boundary and inertial effects need to be accounted for (Vafai 2005). For example, modeling fluid flows in the fuel cells. This is because the fuel cell consists of a number of distinct layers of different porosities. The Darcy law assumes no effect of boundaries and the fluid velocity in Darcy's equation is determined by the permeability of the matrix. Therefore, at the interface between the regions of different porosity in the fuel cell, particularly between the free fluid flow region such as a gas flow channel and a permeable medium, then a discontinuity in the fluid velocity and/or the shear stress could emerge (Ingham and Pop 2005).

Equations (1)–(3) can be written in terms of the stream function ψ defined as $u=\partial\psi/\partial y$ and $v=-\partial\psi/\partial x$ together with the following non-dimensional variables:

$$\Psi=\frac{\nu}{g\beta K\ell\Delta T}\psi,\qquad \Theta_{\mathrm{p}}=\frac{T_{\mathrm{p}}-T_{\mathrm{c}}}{\Delta T},\qquad \Theta_{\mathrm{w}}=\frac{T_{\mathrm{w}}-T_{\mathrm{c}}}{\Delta T},$$
$$X=\frac{x}{\ell},\qquad Y=\frac{y}{\ell},\qquad D=\frac{d}{\ell},\qquad (\text{where } \Delta T=T_{\mathrm{h}}-T_{\mathrm{c}}>0) \tag{5}$$

The resulting non-dimensional forms of the governing Eqs. (1)–(4) are

$$\frac{\partial^2\Psi}{\partial X^2}+\frac{\partial^2\Psi}{\partial Y^2}=\frac{\partial\Theta_{\mathrm{p}}}{\partial Y} \tag{6}$$

$$Ra\left[\frac{\partial\Psi}{\partial Y}\frac{\partial\Theta_{\mathrm{p}}}{\partial X}-\frac{\partial\Psi}{\partial X}\frac{\partial\Theta_{\mathrm{p}}}{\partial Y}\right]=\frac{\partial^2\Theta_{\mathrm{p}}}{\partial X^2}+\frac{\partial^2\Theta_{\mathrm{p}}}{\partial Y^2}+\gamma\Theta_{\mathrm{p}}^{\lambda} \tag{7}$$

$$\frac{\partial^2\Theta_{\mathrm{w}}}{\partial X^2}+\frac{\partial^2\Theta_{\mathrm{w}}}{\partial Y^2}=0 \tag{8}$$

where Ra is the Rayleigh number defined as $Ra=g\beta K\Delta T\ell/(\nu\alpha)$ and γ is the internal heating parameter defined as $\gamma=G\ell(\Delta T)^{\lambda-1}/(\alpha\rho c_{\mathrm{p}})$. The values of the non-dimensional stream function are zero in the wall region and on the solid–fluid interfaces. The boundary conditions for the non-dimensional temperatures are

$$\Theta_{\mathrm{w}}(X,0)=1;\qquad \Theta_{\mathrm{p}}(X,1)=0 \tag{9}$$
$$\partial\Theta_{\mathrm{p}}(0,Y)/\partial X=0;\qquad \partial\Theta_{\mathrm{w}}(0,Y)/\partial X=0 \tag{10}$$
$$\partial\Theta_{\mathrm{p}}(1,Y)/\partial X=0;\qquad \partial\Theta_{\mathrm{w}}(1,Y)/\partial X=0 \tag{11}$$
$$\Theta_{\mathrm{p}}(X,D)=\Theta_{\mathrm{w}}(X,D);\qquad \partial\Theta_{\mathrm{p}}(X,D)/\partial Y=Kr\,\partial\Theta_{\mathrm{w}}(X,D)/\partial Y \tag{12}$$

where $Kr = k_w/k_p$ is the thermal conductivity ratio. The physical quantities of interest in this problem are the average Nusselt number, defined by:

$$\overline{Nu}_w = \int_0^1 \frac{-\partial \Theta_w}{\partial Y}\Big|_{Y=0,D} dY \tag{13}$$

$$\left(\overline{Nu}_p\right)_h = \int_0^1 \frac{-\partial \Theta_p}{\partial Y}\Big|_{Y=D} dY \tag{14}$$

$$\left(\overline{Nu}_p\right)_c = \int_0^1 \frac{-\partial \Theta_p}{\partial Y}\Big|_{Y=1} dY \tag{15}$$

where $\overline{Nu}_w$ is representing the dimensionless heat transfer through the solid wall, $\left(\overline{Nu}_p\right)_h$ and $\left(\overline{Nu}_p\right)_c$ are representing the dimensionless heat transfer through the hot and cold porous walls, respectively.

3 Numerical Method and Validation

An iterative finite difference procedure is employed to solve Eqs. (6)–(8) subject to the boundary conditions (9)–(12). The grid-points distribution at the conducting wall and porous enclosure is shown in Fig. 1b where $ND + 1$ is number of nodal points in the horizontal axis in the wall. The numerical solution will be preceded by giving the finite difference equation (FDE) of the stream function equation (6) and energy equation for the porous (7) and the impermeable wall (8). The FDE of (6) written in the Gaussian SOR formulation is

$$\Psi_{i,j}^{k+1} = \Psi_{i,j}^{k} + \frac{\lambda_r}{2(1+B^2)}\left[\Psi_{i+1,j}^{k} + \Psi_{i-1,j}^{k+1} + B^2\left(\Psi_{i,j+1}^{k} + \Psi_{i,j-1}^{k+1}\right) - 2(1+B^2)\Psi_{i,j}^{k} + (\Delta X)^2 (S_\Psi)_{i,j}^{k}\right] \tag{16}$$

with

$$B = \frac{\Delta X}{\Delta Y}, \qquad (S_\Psi)_{i,j} = \frac{(\Theta_p)_{i,j+1} - (\Theta_p)_{i,j-1}}{2\Delta Y} \tag{17}$$

Similarly (7) can be written as

$$(\Theta_p)_{i,j}^{k+1} = (\Theta_p)_{i,j}^{k} + \frac{\lambda_r}{2(1+B^2)}\left[(\Theta_p)_{i+1,j}^{k} + (\Theta_p)_{i-1,j}^{k+1} + B^2\left((\Theta_p)_{i,j+1}^{k} + (\Theta_p)_{i,j-1}^{k+1}\right) - 2(1+B^2)(\Theta_p)_{i,j}^{k} - (\Delta X)^2 (S_{\Theta_p})_{i,j}^{k}\right] \tag{18}$$

with

$$(S_{\Theta_p})_{i,j} = Ra\left[\left(\frac{\Psi_{i,j+1} - \Psi_{i,j-1}}{2\Delta Y}\right)\left(\frac{(\Theta_p)_{i+1,j} - (\Theta_p)_{i-1,j}}{2\Delta X}\right) - \left(\frac{\Psi_{i+1,j} - \Psi_{i-1,j}}{2\Delta X}\right)\left(\frac{(\Theta_p)_{i,j+1} - (\Theta_p)_{i,j-1}}{2\Delta Y}\right)\right] - \gamma\left(\frac{(\Theta_p)_{i+1,j} + (\Theta_p)_{i-1,j} + (\Theta_p)_{i,j+1} + (\Theta_p)_{i,j-1}}{4}\right)^{\lambda} \tag{19}$$

The FDE of (8) written in Gaussian SOR formulation is

$$(\Theta_{\mathrm{w}})_{i,j}^{k+1} = (\Theta_{\mathrm{w}})_{i,j}^{k} + \frac{\lambda_r}{2(1+B^2)}\left[(\Theta_{\mathrm{w}})_{i+1,j}^{k} + (\Theta_{\mathrm{w}})_{i-1,j}^{k+1} + B^2\left((\Theta_{\mathrm{w}})_{i,j+1}^{k} + (\Theta_{\mathrm{w}})_{i,j-1}^{k+1}\right) - 2(1+B^2)(\Theta_{\mathrm{w}})_{i,j}^{k}\right] \tag{20}$$

The conditions at the interface boundary are

$$\begin{aligned}(\Theta_{\mathrm{p}})_{i,ND+1}^{k+1} &= (\Theta_{\mathrm{w}})_{i,ND+1}^{k} \\ (\Theta_{\mathrm{w}})_{i,ND+1}^{k+1} &= \left[\left(\frac{1}{Kr}\right)\left(-(\Theta_{\mathrm{p}})_{i,ND+3}^{k} + 4(\Theta_{\mathrm{p}})_{i,ND+2}^{k} - 3(\Theta_{\mathrm{p}})_{i,ND+1}^{k}\right)\right. \\ &\quad \left. + 4(\Theta_{\mathrm{w}})_{i,ND}^{k} - (\Theta_{\mathrm{w}})_{i,ND}^{k}\right]/3 \end{aligned} \tag{21}$$

Regular and uniform grid distribution is used for the whole enclosure. The effect of grid resolution was examined in order to select the appropriate grid density as demonstrated in Fig. 2 for $D = 0.1$, $Kr = 2.4$, $\gamma = 0$, and $Ra = 1000$. The results indicate that an 120×120 grid can be used in the final computations. To validate the computation code, the previously published problems on natural convection in a square porous enclosure with/without conductive wall, $Kr = 1$ and no heat source ($\gamma = 0$) were solved. Table 1 shows that the average Nusselt number are in good agreement with the solutions reported by the literatures. These comprehensive verification efforts demonstrated the robustness and accuracy of the present computation.

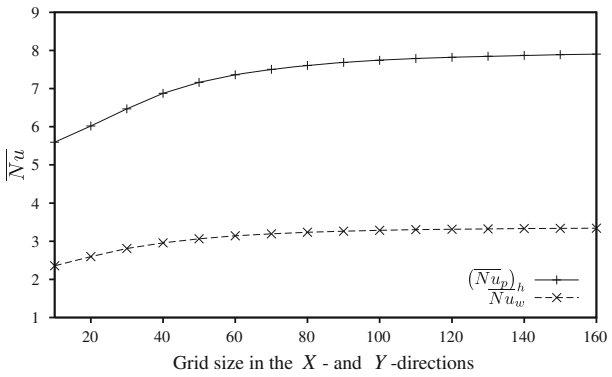

Fig. 2 Grid independency study: $\overline{Nu}$ versus number of grid points at $D = 0.1$, $Kr = 2.4$, $\gamma = 0$, and $Ra = 1000$

Table 1 Comparison of $(\overline{Nu}_{\mathrm{p}})_{\mathrm{h}}$ values with some results from the literature for $Kr = 1$ and $\gamma = 0$

D	Present	Saeid (2007b)	Manole and Lage (1992)	Walker and Homsy (1978)
0	13.342	13.726	13.637	12.96
0.02	9.897	10.041	–	–
0.1	4.926	5.044	–	–
0.2	3.094	3.186	–	–
0.5	1.532	1.566	–	–

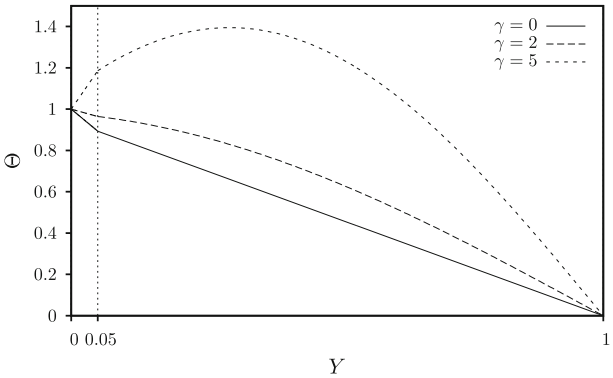

(a) $D = 0.05$, $Kr = 0.44$ and $\gamma = 0, 2, 5$

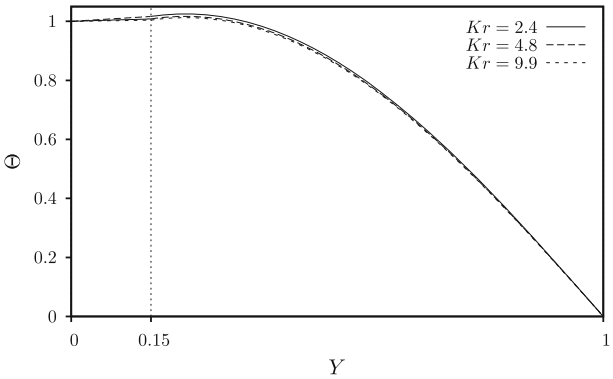

(b) $D = 0.15$, $\gamma = 4$ and $Kr = 2.4, 4.8, 9.9$

Fig. 3 Temperature distribution at $Ra = 0$ and $\lambda = 1$

4 Results and Discussion

The analyses in the undergoing numerical investigation are performed in the following domain of the associated dimensionless groups: the wall thickness, $0.02 \leq D \leq 0.5$; the thermal conductivity ratio, $0.44 \leq Kr \leq 9.9$; the internal heat generated, $0 \leq \gamma \leq 5$; the exponent in the local heating term, $1 \leq \lambda \leq 3$; and the Rayleigh number, $0 \leq Ra \leq 1000$.

When $Ra = 0$ the temperature inside the porous enclosure, Eq. (7), becomes independent of that for the flow, Eq. (6). In this case, the systems PDEs (6)–(8) reduces to the boundary value problem (systems ODEs). Some solutions of this BVPs are plotted in Fig. 3. Figure 3a shows the effects of the internal heat source γ for $D = 0.05$ and $Kr = 0.44$. When no internal heat source inside the porous enclosure, the distribution of temperature is a linear function of Y. The exothermic reaction in the porous material generated more heat causes the fluid temperature rise sharply, this implies the maximum fluid temperature above the conductive solid wall and distribute non-linearly as shown in Fig. 3a. While Fig. 3b shows the effects of the conductivity ratio Kr for $D = 0.15$, $\gamma = 4$. Temperature distribute linearly in the conductive solid wall. Variation Kr has small effect in the temperature distribution inside the porous enclosure. Detail investigation shows that increasing the conductivity ratio

decreases the temperature in the porous enclosure. Increasing Kr values also decreases the temperature in the solid wall as seen in Fig. 3b.

Figure 4 illustrates the effects of the wall thickness parameter D, for $Kr = 2.4$, $\gamma = 4$, $\lambda = 1$, and $Ra = 40$ on the flow fields and thermal fields in the porous enclosure and the solid wall. As can be seen in Fig. 4a–c, the parameter D affects the flow characteristics and the fluid temperatures as well as the solid wall temperatures. Strong internal heat source gives maximum fluid temperature in the porous enclosure more than the heated solid wall. As the wall thickness increases, the $(\Theta_p)_{max}$ decreases significantly and lower than the heated solid wall as shown in Fig. 4b, c. The strength of the flow circulation of the fluid-saturated porous medium is much higher for a thin solid wall. It is important to note that the Rayleigh number in this study is based on the total height of the wall and not on the thickness of the porous layer.

To show the effect of the thermal conductivity ratio Kr on the circulation and the thermal fields of the fluid in the porous enclosure, the streamlines and isotherms are presented in Fig. 5 for $D = 0.2$, $\gamma = 4$, $\lambda = 1$, and $Ra = 40$. Three different materials are selected, which are the epoxy–water ($Kr = 0.44$), glass–water ($Kr = 2.4$), and epoxy–air ($Kr = 9.9$) were used. It observed that the $(\Theta_p)_{max}$ increases by increasing Kr values. The higher values of Kr enhances the flow strength. This phenomenon is happened due to the temperature gradient near the wall increases with the increase of the parameter Kr. Thus, much heat transfer from the solid wall to the porous media is obtained for higher values of Kr (good conductive solid wall). It is also observed in the Fig. 5b, c that convection effects inside the porous medium become stronger for higher values of Kr.

Figure 6a–c shows the effects of Ra on the flow fields and the thermal fields inside the porous enclosure and the solid wall with constant values of $D = 0.2$, $Kr = 2.4$, $\gamma = 4$, and $\lambda = 1$. As can be seen in the isotherms Fig. 6a that temperature distribution slightly distorted as a signed of transition from the conduction to the convection mode. When Ra take higher values as depicted in the isotherms Fig. 6b, c that distribution more distorted as effect of the strength of convection current related with the Ra values. The central vortex of the flow fields widen and toward the cold wall by increasing Ra values. It also observed that $(\Theta_p)_{max}$ and Ψ_{max} decrease as Ra values take higher.

To show the effect of the internal heat source γ on the circulation and thermal fields of the fluid in the porous enclosure, the streamlines, and isotherms are presented in Fig. 7 for $D = 0.2$, $Kr = 2.4$, $\lambda = 1$, and $Ra = 40$. It shows from Fig. 7 that increasing internal heat source increases the flow strength and the maximum fluid temperature. The $(\Theta_p)_{max}$ located away from the interface solid wall. This situation is similar with the Fig. 3a for $Ra = 0$.

Variation of the average Nusselt number along the hot interface and the cold wall with the Rayleigh number is shown in Fig. 8 for different values of the wall thickness D and porous media made of glass–water ($Kr = 2.4$) with $\gamma = 4$ and $\lambda = 1$. Obviously, the heat transfer increases by increasing Ra. The heat transfer enhancement for both the hot interface and the cold wall by increasing Ra is more pronounced at a thin solid wall. The heat transfer becomes constant for the highest values of the wall thickness parameter of the solid wall D. This is due to the conductive solid wall behaves as insulated material in this case. Figure 8 also shows that for a low Ra, increasing the thickness of solid wall increases the heat transfer at the hot interface but the heat transfer decreases at the cold wall.

Variation of the average Nusselt number along the hot interface and the cold wall with the Rayleigh number is shown in Fig. 9 for different values of Kr with constant $D = 0.2$, $\gamma = 4$, and $\lambda = 1$. The result presented in the Fig. 9 shows that the heat transfer remain stable for any values of the thermal conductivity ratio at $Ra < 10$. The heat transfer enhancement by increasing Ra is more pronounced at the higher Kr values. This is due to the temperature

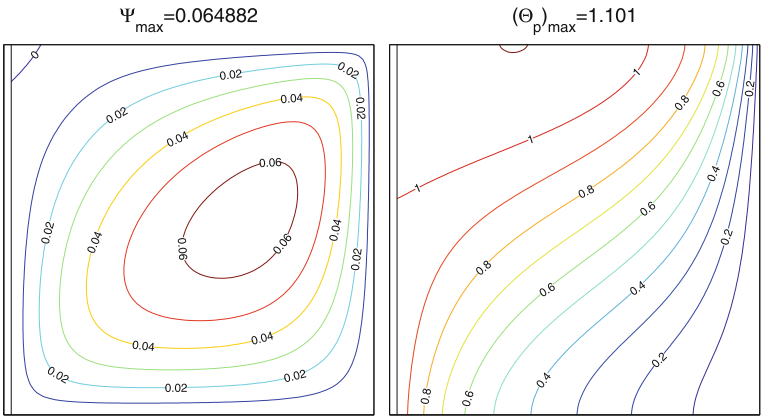

(a) $D = 0.02$

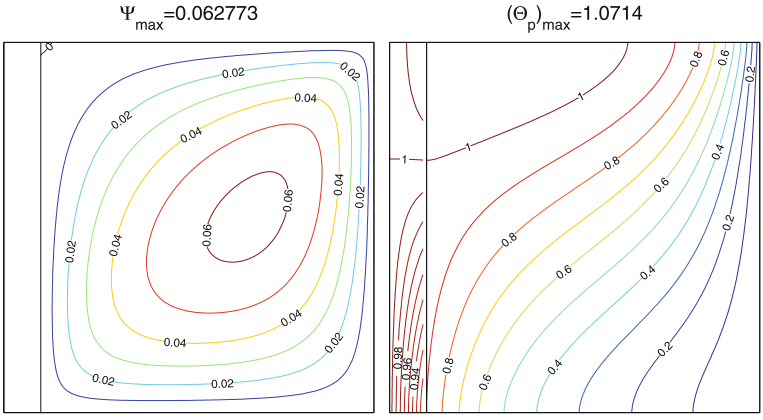

(b) $D = 0.1$

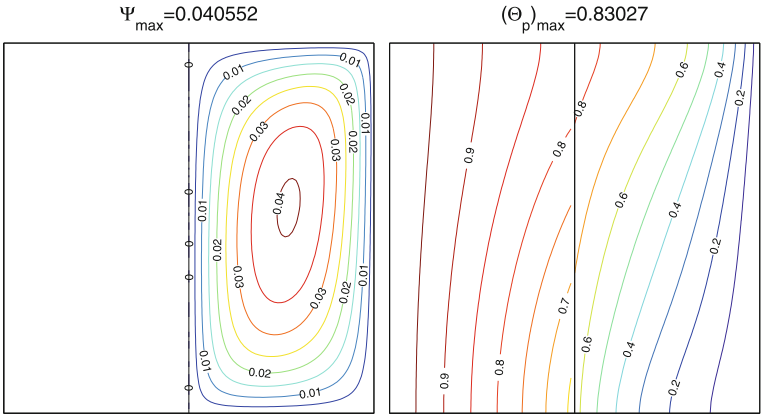

(c) $D = 0.5$

Fig. 4 Streamlines (*left*), isotherms (*right*) at $Ra = 40$, $Kr = 2.4$, $\gamma = 4$, and $\lambda = 1$

gradient near the solid wall increases with increasing Kr as shown in Fig. 5. Although the magnitude of the average Nusselt number on the hot interface and the cold wall are different the heat transfer behavior are similar.

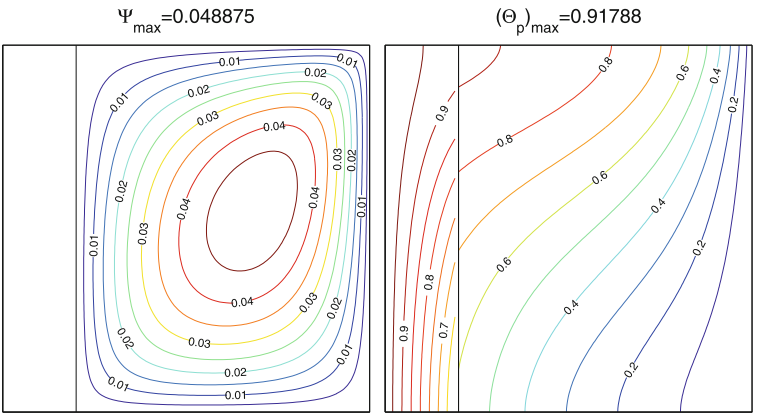

(a) $Kr = 0.44$

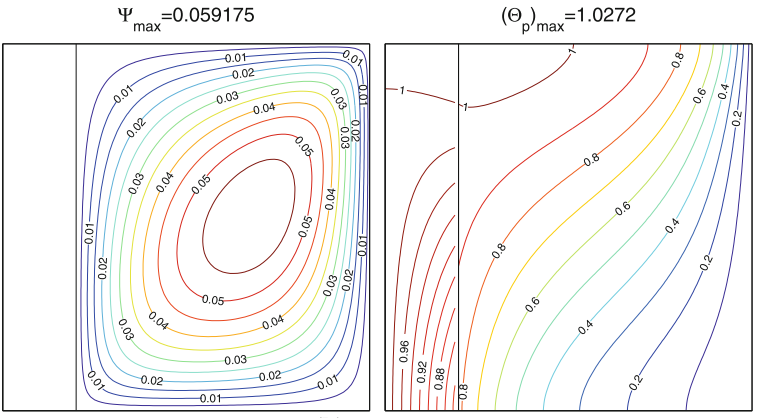

(b) $Kr = 2.4$

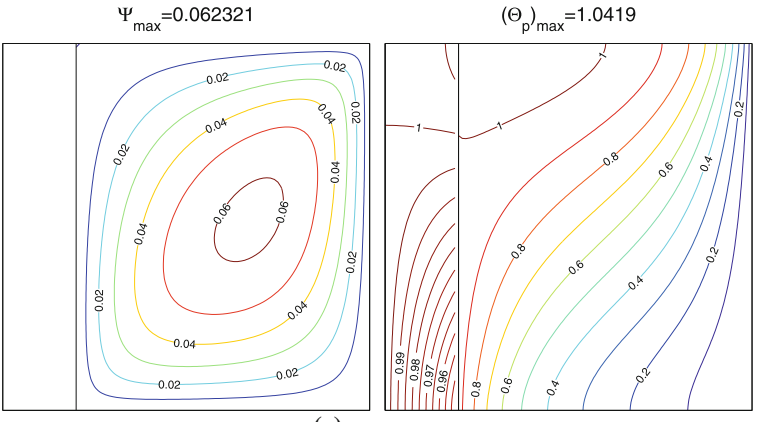

(c) $Kr = 9.9$

Fig. 5 Streamlines (*left*), isotherms (*right*) at $Ra = 40$, $D = 0.2$, $\gamma = 4$, and $\lambda = 1$

The variation of the average Nusselt number along the hot interface and the cold wall with the Rayleigh number is shown in Fig. 10 for the combinations values of γ and λ with constant $D = 0.2$ and $Kr = 2.4$. The result presented in the Fig. 9 shows that the heat

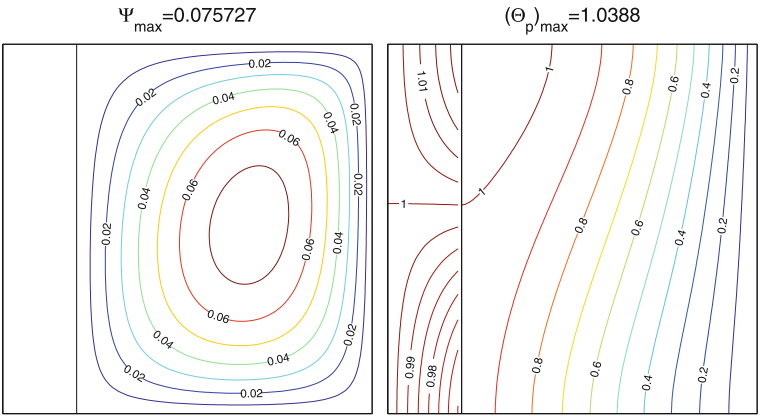

(a) $Ra = 10$

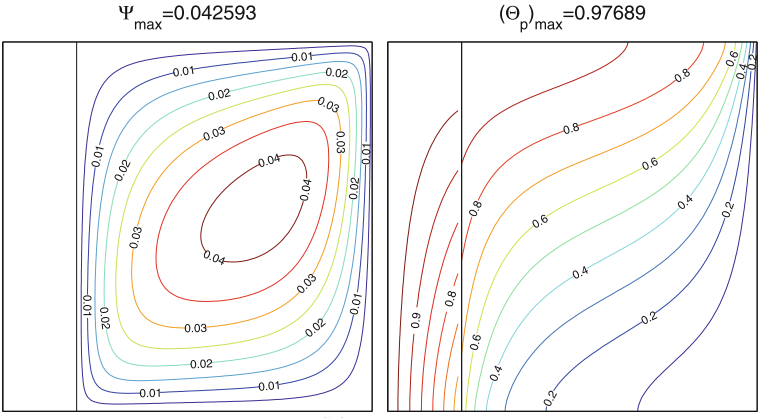

(b) $Ra = 100$

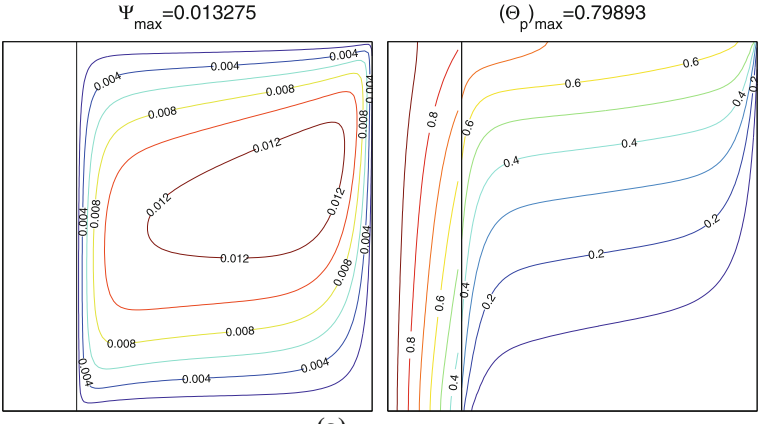

(a) $Ra = 1000$

Fig. 6 Streamlines (*left*), isotherms (*right*) at $D = 0.2,\ Kr = 2.4,\ \gamma = 4$, and $\lambda = 1$

transfer rate at the hot interface and the cold wall are exactly equal when no internal heat source ($\gamma = 0$). For a fixed Ra, increasing γ decreases the $\left(\overline{Nu}_{\mathrm{p}}\right)_{\mathrm{h}}$ but increase the $\left(\overline{Nu}_{\mathrm{p}}\right)_{\mathrm{c}}$.

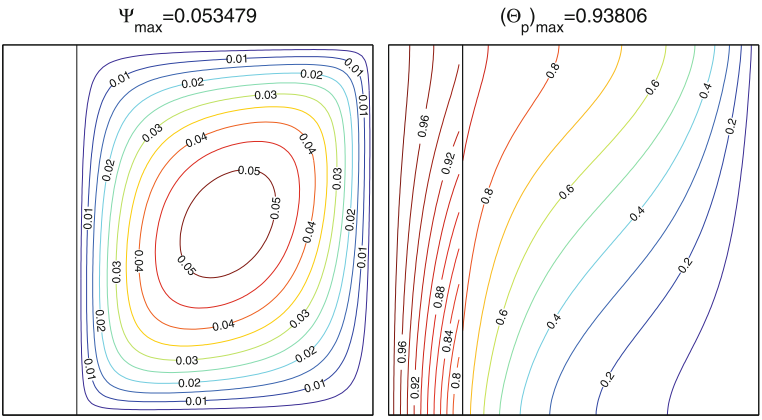

(a) $\gamma = 0$

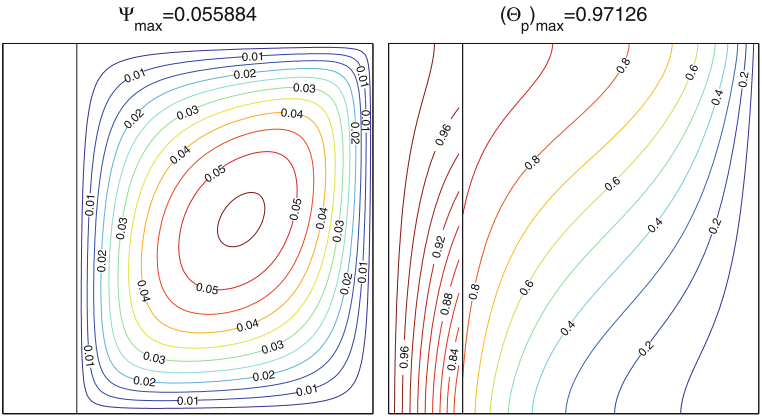

(b) $\gamma = 2$

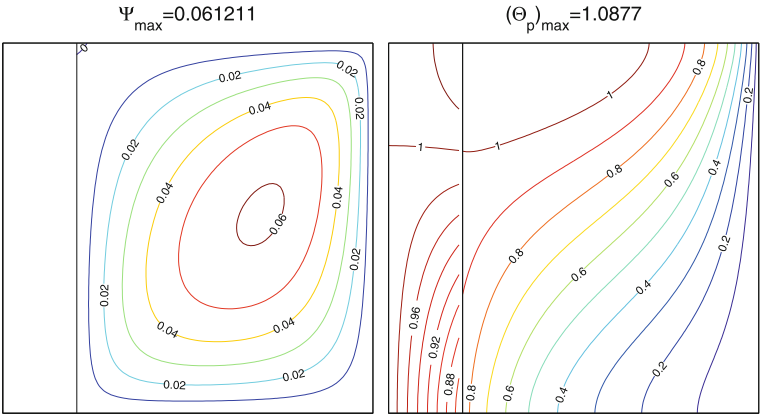

(c) $\gamma = 5$

Fig. 7 Streamlines (*left*), isotherms (*right*) at $D = 0.2,\ Kr = 2.4,\ \lambda = 1$, and $Ra = 40$

Figure 10 also shows that the heat transfer rate is significantly modified by varying the local heating exponent λ.

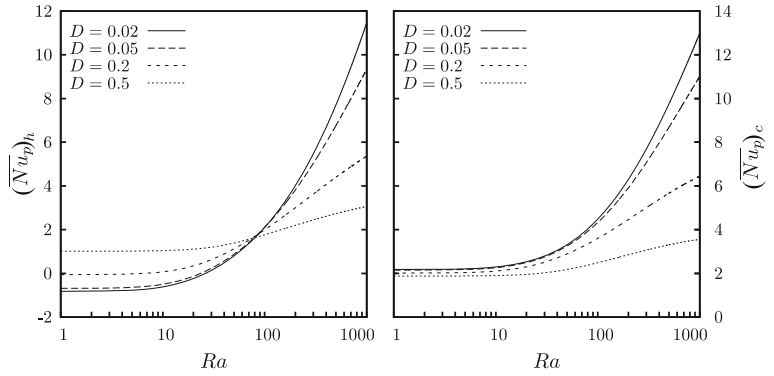

Fig. 8 Variation of the average Nusselt number along the hot interface (*left*) and the cold wall (*right*) with Ra for different D

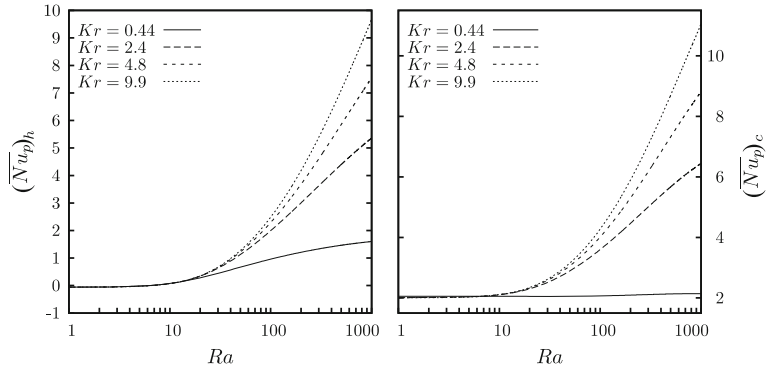

Fig. 9 Variation of the average Nusselt number along the hot interface (*left*) and the cold wall (*right*) with Ra for different Kr

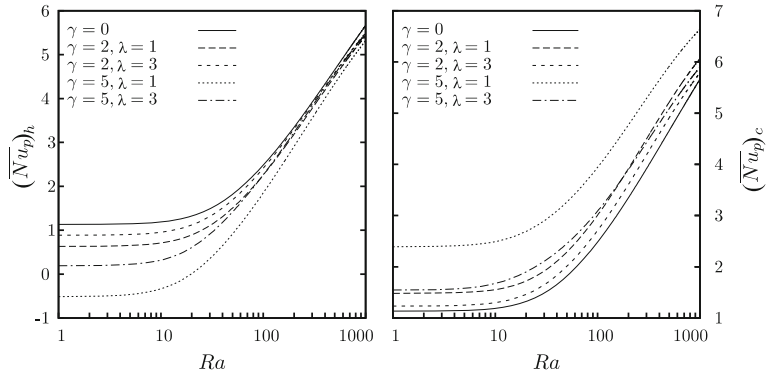

Fig. 10 Variation of the average Nusselt number along the hot interface (*left*) and the cold wall (*right*) with Ra for different Kr

5 Conclusions

The present numerical simulation study the effects of a conductive wall on natural convection in a square porous enclosure having internal heating at a rate proportional to the local temperature difference. The dimensionless forms of the governing equations are solved using the finite difference method. Detailed computational results for flow and temperature field and the heat transfer rate in the enclosure have been presented in the graphical form. The main conclusions of the present analysis are as follows:

1. Strong internal heating can generate significant maximum fluid temperature more than the conductive solid wall. Increasing value thermal conductivity ratio and/or decreasing the thickness of solid wall can increase the maximum fluid temperature.
2. The strength of the flow circulation of the fluid saturated the porous medium is much higher with thin walls and/or a higher value of the solid to fluid thermal conductivity ratio. The internal heat generation made the strength of the flow circulation weaken by Increasing Rayleigh number
3. The heat transfer remain stable for any values of the thermal conductivity ratio at very low Rayleigh number.

References

Al-Amiri, A., Khanafer, K., Pop, I.: Steady-state conjugate natural convection in a fluid-saturated porous cavity. Int. J. Heat Mass Transf. **51**, 4260–4275 (2008)

Baytas, A.C., Liaqat, A., Grosan, T., Pop, I.: Conjugate natural convection in a square porous cavity. Heat Mass Transf. **37**, 467–473 (2001)

Chang, W.J., Lin, H.C.: Natural convection in a finite wall rectangular cavity filled with an anisotropic porous medium. Int. J. Heat Mass Transf. **37**, 303–312 (1994a)

Chang, W.J., Lin, H.C.: Wall heat conduction effect on natural convection in an enclosure filled with a non-darcian porous medium. Numer. Heat Transf. A **25**, 671–684 (1994b)

de Lemos, M.J.S.: Turbulence in Porous Media: Modeling and Applications. Elsevier, Oxford (2006)

Haajizadeh, M., Ozguc, A.F., Tien, C.L.: Natural convection in a vertical porous enclosure with internal heat generation. Int. J. Heat Mass Transf. **27**, 1893–1902 (1984)

Ingham, D.B, Pop, I.: Transport Phenomena in Porous Media. Elsevier Science, Oxford (1998)

Ingham, D.B., Bejan, A., Mamut, E., Pop, I.: Emerging Technologies and Techniques in Porous Media. Kluwer, Dordrecht (2004)

Ingham, D.B., Pop, I.: Transport Phenomena in Porous Media III. Elsevier Science, Oxford (2005)

Joshi, M.V., Gaitonde, U.N., Mitra, S.K.: Analytical study of natural convection in a cavity with volumetric heat generation. J. Heat Transf. **128**, 176–182 (2006)

Manole, D.M., Lage, J.L.: Numerical benchmark results for natural convection in a porous medium cavity, in: Heat and mass transfer in porous media. ASME HTD **216**, 55–60 (1992)

Mealey, L.R., Merkin, J.H.: Steady finite Rayleigh number convective flows in a porous medium with internal heat generation. Int. J. Therm. Sci. **48**, 1068–1080 (2009)

Nield, D.A., Bejan, A.: Convection in Porous Media, 3rd edn. Springer, New York (2006)

Pop, I., Ingham, D.B.: Convective Heat Transfer: Mathematical and Computational Modelling of Viscous Fluids and Porous Media. Pergamon, Oxford (2001)

Rao, Y.F., Wang, B.X.: Natural convection in vertical porous enclosures with internal heat generation. Int. J. Heat Mass Transf. **34**, 247–252 (1991)

Saeid, N.H.: Conjugate natural convection in a vertical porous layer sandwiched by finite thickness walls. Int. Commun. Heat Mass Transf. **34**, 210–216 (2007a)

Saeid, N.H.: Conjugate natural convection in a porous enclosure: effect of conduction in one of the vertical walls. Int. J. Therm. Sci. **46**, 531–539 (2007b)

Saeid, N.H.: Conjugate natural convection in a porous enclosure sandwiched by finite walls under thermal nonequilibrium conditions. J. Porous Media **11**, 259–275 (2008)

Saleh, H., Saeid, N.H., Hashim, I., Mustafa, Z.: Effect of conduction in bottom wall on Darcy-Bénard convection in a porous enclosure. Transp. Porous Media **88**, 357–368 (2011)

Vadasz, P.: Emerging Topics in Heat and Mass Transfer in Porous Media. Springer, New York (2008)
Vafai, K.: Handbook of Porous Media, 2nd edn. Taylor and Francis, New York (2005)
Varol, Y., Oztop, H.F., Koca, A.: Entropy generation due to conjugate natural convection in enclosures bounded by vertical solid walls with different thicknesses. Int. Commun. Heat Mass Transf. **35**, 648–656 (2008)
Varol, Y., Oztop, H.F., Mobedi, M., Pop, I.: Visualization of heat flow using Bejan's heatline due to natural convection of water near 4°C in thick walled porous cavity. Int. J. Heat Mass Transf. **53**, 1691–1698 (2010)
Walker, K.L., Homsy, G.M.: Convection in porous cavity. J. Fluid Mech. **87**, 449–474 (1978)